I&EC research
Industrial & Engineering Chemistry Research

pubs.acs.org/IECR
Article

HHDH-Catalyzed Synthesis of Enantioenriched Fluorinated β-Hydroxy Nitrile—Process Advances through a Reaction Engineering Approach

Nevena Milčić, Martina Sudar, Ana-Katarina Marić, Krešimir Kos, Maja Majerić Elenkov, and Zvjezdana Findrik Blažević*

Cite This: *Ind. Eng. Chem. Res.* 2024, 63, 7051−7063

ABSTRACT: This study explores halohydrin dehalogenase (HHDH) variant ISM-4 for the synthesis of enantioenriched fluorinated β-hydroxy nitrile, focusing on the reaction engineering perspective for the enhancement of process metrics. Detailed kinetic assessments, enzyme affinities, inhibitions, and deactivation dependency are integrated into a mathematical model, providing insights into ISM-4 limitations and optimal conditions for (*S*)-3-(4-fluorophenyl)-3-hydroxypropanenitrile's synthesis. By strategically feeding the substrate in a fed-batch or a repetitive-batch reactor, substantial improvements are achieved compared to the batch reactor, yielding the 75 and 145 mM desired product with ee > 90 and 80%, respectively. Additionally, findings from in silico simulations guided the selection of process conditions for a reaction on a 100 mL scale in a rotating-bed reactor with an immobilized catalyst, resulting in the 24.7 mM product (*Y* = 72%, ee 92%). This study highlights the important role of a reaction engineering approach in enhancing HHDH-catalyzed synthesis for scalable production of valuable enantioenriched building blocks.

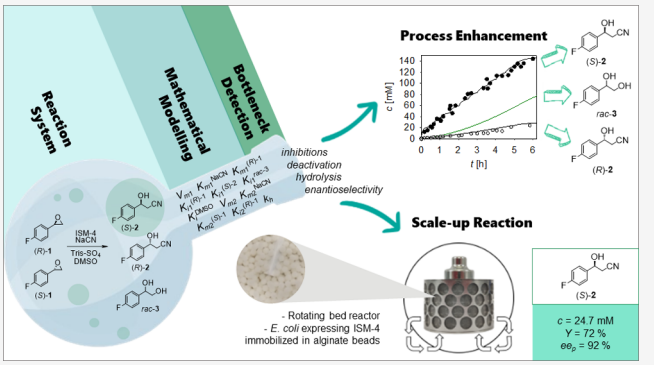

1. INTRODUCTION

Optically pure β-hydroxy nitriles are versatile building blocks in pharmaceutical and fine chemical industries.[1,2] The cyano group in a molecule is an essential synthon for further transformation to diverse classes of synthetically essential compounds, such as amides, amines, amino acids, and carboxylic acids.[3] As biological target molecules are sophisticated selectors regarding chirality, optical purity increases the value of intermediates for the synthesis of APIs.[4] Optically pure β-hydroxy nitriles are a part of the production path toward antidepressants, β-blockers, statins, etc.[5−8] Their importance further increases when molecules are not only optically active but contain fluorinated moieties, which can drastically enhance biochemical properties of great importance for drug design.[2,9] Since direct fluorination is challenging from both economic and environmental perspectives, the development of sustainable methods for modifying existing fluorinated synthons is a valuable alternative.[10,11] This work addresses the reaction engineering perspective of the biocatalytic synthesis of (*S*)-3-(4-fluorophenyl)-3-hydroxypropanenitrile ((*S*)-**2**) and (*S*)-2-(4-fluorophenyl)oxirane ((*S*)-**1**) catalyzed by a halohydrin dehalogenase (HHDH) variant (Scheme 1). HHDHs, involved in the reversible dehalogenation of vicinal halohydrins and the formation of epoxides, are synthetically valuable candidates because of their activity, enantioselectivity, and diversity of accepting nucleophiles in ring-opening reactions.[12−18] Their importance is best depicted by the use of HHDH members in the industrial production of atorvastatin, the active ingredient of the cholesterol-lowering drug Lipitor (Pfizer), and a key intermediate for (*S*)-cidofovir, the antiviral drug Vistide (Gilead Sciences).[19,20]

Depending on the reaction system studied and the HHDH candidate employed, epoxide ring-opening reactions may occur in a completely enantioselective fashion, whereby kinetic resolutions result in higher-value products, i.e., optically pure β-substituted alcohols and unreacted enantiomers of the substrates.[14] However, the biocatalytic synthesis of enantiopure compounds becomes more complex when the enzyme accepts both enantiomers in the reactions. Some of the catalytic and structural properties of enzymes, including enantiopreference, can be introduced or enhanced by protein engineering methods.[21,22] Following this concept, the thermo-

Received: February 4, 2024
Revised: April 1, 2024
Accepted: April 3, 2024
Published: April 12, 2024

https://doi.org/10.1021/acs.iecr.4c00477
Ind. Eng. Chem. Res. 2024, 63, 7051−7063

Scheme 1. Synthesis of (*S*)-2 through the ISM-4-Catalyzed *rac*-1 Ring-Opening Mediated by Cyanide Ions

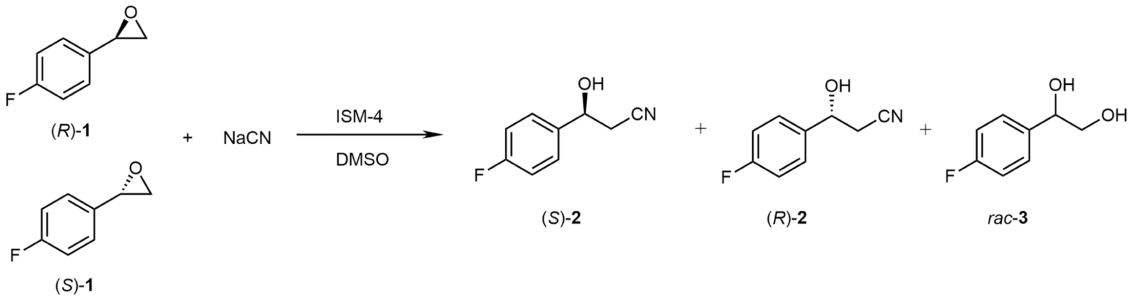

stable ISM-4 variant was obtained in previous research by the combinatorial directed evolution strategy.[23] In the respective research, the variant was characterized in terms of temperature vs activity profile, thermal denaturation, and half-life value (T_m = 73 °C, $t_{1/2}^{65\,°C}$ = 51 h). Compared to the wild-type HheC, ISM-4 displayed increased thermal stability and superior resistance when subjected to the action of organic solvents, accompanied by improved, although not absolute, enantioselectivity.[24] As this enzyme variant proved to be a promising and robust candidate for the synthesis under demanding reaction conditions,[24] in this work, the potential of ISM-4 for the production of optically active compounds was further evaluated. The enzyme variant was subjected to kinetic characterization in cyanolysis of *rac*-**1** (Scheme 1), with a special emphasis on the differences between its catalytic activities toward enantiomers of the substrate. The main goal was finding the conditions that will enable the synthesis of the product in highly enantioenriched form by employing a bioreaction engineering approach. The application of reaction engineering principles plays a decisive role in choosing reaction conditions for enhanced efficiency and selectivity. Mathematical models offer not only valuable insights into the kinetics of catalyzed reactions, leading to a better overall understanding of the occurring processes but also support the design and optimization of reaction systems, with the final goal of facilitating the processes scale-up for industrial applications.[25−28]

2. MATERIALS AND METHODS

2.1. Materials. Commercially available chemicals were purchased from suppliers and used without further processing: Acros Organics (Belgium)—tris(hydroxymethyl)-aminomethane (Tris); Fisher Scientific (USA)—dimethyl sulfoxide (DMSO), methanol (MeOH), acetonitrile (MeCN), ethyl acetate (EtOAc), *n*-hexane, isopropanol (*i*-PrOH), and *rac*-2-(4-fluorophenyl)oxirane (*rac*-**1**); abcr GmbH (Germany)—(*R*)-2-(4-fluorophenyl)oxirane ((*R*)-**1**); Carl Roth (Germany)—arabinose, ethylenediaminetetraacetic acid (EDTA), Luria−Bertani broth, agar, and ampicillin; Sigma-Aldrich Corporation (SAD)—calcium lactate pentahydrate and sodium sulfate; Roche (Switzerland)—protease inhibitor cOmplete, and Honeywell Fluka (USA)—sodium acetate, sodium alginate. Commercially unavailable chemicals were synthesized with respect to the following protocols: *para*-nitro-2- bromo-1-phenylethanol (PNSHH) and *para*-nitro styrene oxide (PNSO),[29] 3-(4-fluorophenyl)-3-hydroxypropanenitrile (*rac*-**2**),[30] and *rac*-1-(4-fluorophenyl)-1,2-ethanediol (*rac*-**3**).[31] Synthetic procedures for (*S*)-2-(4-fluorophenyl)-oxirane ((*S*)-**1**) and (*R*)-3-(4-fluorophenyl)-3-hydroxypropanenitrile ((*R*)-**2**) are given in the Supporting Information (Protocol S1, SI). The plasmid for the ISM-4 variant was kindly provided by the Tang group,[23] and the enzyme was produced as described below.

2.2. Enzyme Preparation and Characterization. The ISM-4 variant was produced as described in previous research.[23] Briefly, the enzyme was produced by overexpression in *Escherichia coli* MC1061 in an Luria−Bertani medium induced by arabinose. After cell harvest by centrifugation (5000 rpm, 15 min, 4 °C) and disruption by sonication in TEMG buffer (10 mM Tris−SO_4 pH 7.5, 1 mM EDTA, 1 mM β-mercaptoethanol, 10% glycerol), the cell-free extract (CFE) was separated from the remaining cell debris by the second round of centrifugation (11 000 rpm, 40 min, 4 °C) and employed in further experiments. The total protein concentration in CFE was determined by Bradford protein assay,[32] while ISM-4's presence in CFE was confirmed by PNSHH assay (see Section 2.5.2 and Scheme S1, SI) and sodium dodecyl-sulfate polyacrylamide gel electrophoresis (SDS-PAGE) electrophoresis (Figure S1, SI).

2.3. HPLC and GC Analyses. *2.3.1. Instruments.* Substrate and product concentrations were monitored on two chromatographs, LC-40 Nexera Lite with a PDA detector from Shimadzu (Japan) and GC-2014 with an FID from Shimadzu (Japan). Conditions, columns, and mobile phases are given below, while details about gradient analyses, retention times, chromatograms, and calibration curves are provided in Figures S2−S5, SI.

2.3.2. PNSHH and PNSO Monitoring. Concentrations of activity assay compounds were monitored via HPLC (flow rate 1.5 mL/min, λ = 310 nm, oven temperature 30 °C) on a Kinetex Core−shell C18 column (2.6 μm, 100 mm × 4.6 mm; Phenomenex, USA) with mobile phase A (80% v/v MeCN, 20% v/v UPW, 0.1% v/v TFA) and B (UPW with 0.1% v/v TFA) (Figure S2, SI).

2.3.3. Achiral Analysis of 1 and 2. Achiral analyses of reaction compounds were performed via HPLC with PDA (flow rate 1 mL/min, λ = 190 nm, oven temperature 30 °C) on a Kinetex Core−shell C18 column (2.6 μm, 100 mm × 4.6 mm; Phenomenex, USA) with mobile phase A (90% v/v MeCN, 10% v/v UPW) and B (UPW) (Figure S3, SI).

2.3.4. Chiral Analysis of (R)-1 and (S)-1. Chiral analyses of substrate enantiomers were performed via GC with FID (flow rate 14.8 mL/min, p = 39.4 kPa, $T_{injector}$ = 250 °C, T_{FID} = 300 °C) on a Lipodex E (50 m × 0.25 mm; Macherey-Nagel, Germany) with N_2 as gas carrier (Figure S4, SI)

2.3.5. Chiral Analysis of (R)-2 and (S)-2. Chiral analyses of product enantiomers were performed via HPLC with PDA (flow rate 1 mL/min, λ = 254 nm, oven temperature 30 °C) on a Chiralpak IC-3 (3 μm, 150 mm × 4.6 mm; Daicel, Japan)

https://doi.org/10.1021/acs.iecr.4c00477
Ind. Eng. Chem. Res. 2024, 63, 7051−7063

with *n*-hexane with 5% v/v *i*-PrOH as mobile phase (Figure S5, SI).

2.4. Kinetic Characterization. Although the reaction system (Scheme 1) can theoretically be divided into three individual reactions (Scheme S2, SI), in reality, all reactions occur simultaneously when *rac*-**1** cyanolysis is performed. To fully and accurately characterize the reaction system, detailed kinetic measurements were performed for each of the reactions separately. The effect of an individual compound on the reaction rate was investigated by varying its concentration while keeping all of the other concentrations and the conditions constant in order to exclude their influence. Although not all compounds are reacting in every reaction step, the effect of each compound on the kinetics of both enzymatic reactions was investigated. For example, not only was the chemical formation of *rac*-**3** (Scheme S2C, SI) with respect to substrate *rac*-**1** concentration kinetically characterized, but also the effect of *rac*-**3** on enzyme specific activity in reactions forming (*S*)-**2** and (*R*)-**2** was evaluated. In addition to all substrates and products, the influence of the range of DMSO concentrations on the specific enzyme activity was also assessed. Since *rac*-**1** solubility in water is as low as 0.26 g L^{-1} at 25 °C,[33] an organic cosolvent is added to the reaction mixture to achieve better substrate solubility and thus increase its bioavailability. DMSO was chosen as a cosolvent based on our previous research regarding suitable media for HHDH-catalyzed biotransformations.[24,34] All of the kinetic experiments were performed in a ThermoMixer C (Eppendorf, Germany) in Eppendorf tubes as reactors under constant common conditions (V_r = 500 μL, 500 mM Tris−SO_4 buffer pH 7.5 at 25 °C, 10% v/v DMSO, 1000 rpm). The individual specific reaction conditions, i.e., the ranges of varying and constant concentrations for each set of kinetic experiments, were selected as follows: NaCN 0−160 mM ($c_{(R)\text{-}1}$ = 10 mM, $\gamma_{ISM\text{-}4}$ = 0.044 mg/mL); (*R*)-**1** 0−85 mM (c_{NaCN} = 80 mM, $\gamma_{ISM\text{-}4}$ = 0.044 mg/mL); (*S*)-**2** 0−30 mM ($c_{(R)\text{-}1}$ = 10 mM, c_{NaCN} = 100 mM, $\gamma_{ISM\text{-}4}$ = 0.044 mg/mL); *rac*-**3** 0−40 mM ($c_{(R)\text{-}1}$ = 10 mM, c_{NaCN} = 100 mM, $\gamma_{ISM\text{-}4}$ = 0.044 mg/mL); DMSO 0−6.8 M ($c_{(R)\text{-}1}$ = 10 mM, c_{NaCN} = 100 mM, $\gamma_{ISM\text{-}4}$ = 0.044 mg/mL); NaCN 0−170 mM ($c_{(S)\text{-}1}$ = 10 mM, $\gamma_{ISM\text{-}4}$ = 0.131 mg/mL); (*S*)-**1** 0−50 mM (c_{NaCN} = 50 mM, $\gamma_{ISM\text{-}4}$ = 0.131 mg/mL); (*R*)-**1** 0−30 mM ($c_{(S)\text{-}1}$ = 10 mM, c_{NaCN} = 80 mM, $\gamma_{ISM\text{-}4}$ = 0.131 mg/mL); *rac*-**1** 0−10 mM concentration effect on its hydrolytic degradation. Kinetic characterization was performed by the initial reaction rate method, which, in practice, means that product formation was observed within the first 10% conversion of the substrate. The reaction mixture was sampled at least 5 times within the initial part of the reaction, taking into account that no more than 10% of the reactor volume is withdrawn in order to maintain the representativeness of the samples. Aliquots of 10 μL were immediately mixed with 500 μL of EtOAc, and extraction was performed by vortexing for 20 s on a Vortex V-1 Plus (Biosan, Latvia). Upon phase separation, the upper organic layer was additionally dried by passing through the layer of Na_2SO_4. Samples prepared in such a manner were subjected to chromatographic analysis as described above (see Section 2.3).

2.5. Stability Measurements. *2.5.1. Setup for Enzyme Stability Measurements.* Except for enzyme activity during biotransformation, the kinetic stability of the enzyme represents a crucial property. The kinetic stability of the enzyme was assessed at resting conditions (i.e., enzyme stability during incubation with individual compounds) and operational conditions (i.e., enzyme operational stability during catalytic activity). All of the stability experiments were conducted on a ThermoMixer C (Eppendorf, Germany) in Eppendorf tubes as reactors under the following constant common conditions: V_r = 500 μL, 500 mM Tris−SO_4 buffer pH 7.5 at 25 °C, 10% v/v DMSO, 1000 rpm. Other conditions (i.e., reaction mixture composition and respective concentrations) differed depending on the studied incubation/reaction, and are described below. To assess enzyme stability during resting time, the enzyme solution ($\gamma_{ISM\text{-}4}$ = 1 mg/mL) was incubated at the common conditions given above and at different concentrations of substrates, that is, *rac*-**1** (0, 5, 20, and 50 mM) or sodium cyanide (0, 20, 50, and 100 mM). Incubation with substrates was never performed with both *rac*-**1** and NaCN at the same time as to avoid an enzymatic reaction between these two substrates. In order to determine the stability of the enzyme without the influence of reaction compounds, the enzyme solution was incubated in a buffer medium without the addition of either of the substrates. During the incubation study, the enzyme was regularly sampled from the incubation medium, diluted in buffer, and separated from the rest of the reaction mixture on Amicon Ultra-0.5 centrifugal units (Merck, USA; 4 °C, 14 000 rpm during 5 min). To ensure complete separation of the enzyme from the rest of the incubation medium, the washing and centrifugation steps were repeated 3 times. Finally, the enzyme was resuspended and fully recovered from the centrifugal unit, whereby the buffer amount was adjusted to correspond to a final CFE concentration of 1 mg/mL. Similarly, during model validation and performance of batch experiments (see Section 2.6), not only substrate consumption and product formation were followed, but also the operational stability of the enzyme. The reaction mixtures were prepared as described in Figure 3 and sampled at regular time intervals. The enzyme preparation for the assay was performed in the same manner as described above for the incubation studies, that is, by successive cycles of washing and centrifugation, finally followed by the full recovery from the centrifugal unit. The enzyme stability, both in the resting and the operational state, was monitored by initiating the individual activity assays in certain time intervals with the separated enzyme solutions.

2.5.2. Activity Assay. ISM-4 activity at certain time points was measured using the assay described previously.[29,35] Briefly, the enzymatic transformation of *para*-nitro-2-bromo-1-phenylethanol (PNSHH) to *para*-nitro styrene oxide (PNSO) (Scheme S1, SI) was monitored using the initial reaction rate method, whereby the reaction mixture was sampled 5 times within 10% conversion of the substrate. Reactions were performed in Eppendorf tubes on a ThermoMixer C (Eppendorf, Germany) under common conditions: V_r = 500 μL, c_{PNSHH} = 5 mM, $\gamma_{ISM\text{-}4}$ = 0.1 mg/mL, 100 mM Tris−SO_4 buffer pH 7.5 at 25 °C, 5% v/v DMSO, and 1000 rpm. Samples from the reaction mixture (10 μL) were diluted in MeCN (390 μL) and filtered through a 0.22 μm filter Chromafil Xtra H-PTFE (Macherey-Nagel, Germany). The concentrations of PNSHH and PNSO were determined by HPLC analysis (see Section 2.3.2).

2.5.3. Enzyme Stability Quantification. Based on the results of the initial reaction rates obtained by the activity assay, the specific enzyme activities were calculated via eq 1. From the activity decline, that is, the drop in the obtained enzymatic activity over time, operational stability decay rate constants (k_d) were estimated under the assumption that the

https://doi.org/10.1021/acs.iecr.4c00477
Ind. Eng. Chem. Res. 2024, 63, 7051−7063

Table 1. Developed Mathematical Model for *rac*-2-(4-Fluorophenyl)oxirane Cyanolysis Catalyzed by the ISM-4 Variant

Kinetic equations		Mass-balance equations	
$r_1 = \frac{V_{m1} \cdot e^{-k_d \cdot t} \cdot c_{(R)-1} \cdot c_{NaCN} \cdot \gamma_{ISM-4}}{\left(K_{m1}^{NaCN} + c_{NaCN}\right) \cdot \left(K_{m1}^{(R)-1} \cdot \left(1 + \frac{c_{(S)-2}}{K_{i1}^{(S)-2}} + \frac{c_{rac-3}}{K_{i1}^{rac-3}} + \frac{c_{DMSO}}{K_i^{DMSO}}\right) + c_{(R)-1} + \frac{c_{(R)-1}^2}{K_{i1}^{(R)-1}}\right)}$	(3)	$\frac{dc_{(R)-1}}{dt} = -0.5 \cdot r_h - r_1$	(6)
$r_2 = \frac{V_{m2} \cdot e^{-k_d \cdot t} \cdot c_{(S)-1} \cdot c_{NaCN} \cdot \gamma_{ISM-4}}{\left(K_{m2}^{NaCN} + c_{NaCN}\right) \cdot \left(K_{m2}^{(S)-1} \left(1 + \frac{c_{(R)-1}}{K_{i2}^{(R)-1}} + \frac{c_{DMSO}}{K_i^{DMSO}}\right) + c_{(S)-1}\right)}$	(4)	$\frac{dc_{(S)-1}}{dt} = -0.5 \cdot r_h - r_2$	(7)
$r_h = k_h \cdot c_{rac-1}$	(5)	$\frac{dc_{NaCN}}{dt} = -r_1 - r_2$	(8)
Operational stability decay		$\frac{dc_{(S)-2}}{dt} = r_1$	(9)
$V_m = V_{m0} \cdot e^{-k_d \cdot t}$	(12)	$\frac{dc_{(R)-2}}{dt} = r_2$	(10)
$k_d = \frac{c_{0,rac-1} \cdot a}{c_{0,rac-1} + b}$	(13)	$\frac{dc_{rac-3}}{dt} = r_h$	(11)

process follows first-order kinetics (eq 2). The estimation of the stability constants was performed within SCIENTIST software, as described below (see Section 2.7).[36]

$$\text{S. A.} = \frac{dc_{PNSO}}{dt} \cdot \frac{1}{\gamma_E} \quad (1)$$

$$\frac{d\gamma_{ISM-4}}{dt} = -k_d \cdot \gamma_{ISM-4} \quad (2)$$

2.6. Batch-Reactor Experiments and Mathematical Model Validation. To confirm the accuracy and applicability of the developed mathematical model, model validation experiments were conducted. Experiments were carried out at common constant conditions (V_r = 1000 μL, 500 mM Tris–SO_4 buffer pH 7.5 at 25 °C, 10% v/v DMSO, 1000 rpm) and different initial concentrations of substrates and the enzyme, whereby the exact composition for each experiment is shown in the description of Figure 3. In the case of the batch reactor, the reaction was initiated by the addition of ISM-4 and monitored for 24 h, both in terms of concentrations of the reaction mixture compounds and the decay of the enzyme operational stability. In the case of the repetitive-batch reactor, 50 mM *rac*-**1** and 25 mM NaCN were added to the reactor every 30 min in 12 portions, while the monitoring proceeded in the same manner as in the case of the batch experiments. Sampling of the reaction mixture was carried out at regular time intervals during 24 h or, in the case of the repetitive-batch experiment, 6 h. The enzyme samples were processed and subjected to activity measurements (see Section 2.5), while the extracted and dried samples were analyzed chromatographically to obtain data on substrate consumption and product formation (see Section 2.3).

2.7. Data Analysis and Development of the Mathematical Model. Data analysis was performed by using program package SCIENTIST.[36] The differential equations were solved using the EPISODE stiff equation package within SCIENTIST software. The selected integrator method uses a relative step size of 0.01, with a maximum allowance of 5000 steps. A relative error tolerance of 1.00×10^{-6} was applied during the numerical integration process, and the solver utilized an analytic Jacobian.[36] The apparent kinetic parameters were estimated from the experimental data sets obtained by the initial reaction rates. The explanation of the method applied for parameter estimation is provided together with Table S1, SI. The data were processed by employing nonlinear regression methods available within the software, i.e., simplex fit or least-squares fit. The hydrolytic decomposition of **1** was described with pseudo-first-order kinetics (Table 1, eq 5) since water participating in the reaction is in such excess that it can be considered part of the hydrolytic constant (k_h). The synthesis of (*S*)-**2** is described by double-substrate Michaelis–Menten kinetics (CN^- and (*R*)-**1** as substrates) with competitive inhibitions by (*S*)-**1**, (*S*)-**2**, *rac*-**3**, DMSO, and substrate inhibition by (*R*)-**1** (Table 1, eq 3). Synthesis of (*R*)-**2** is described by double-substrate Michaelis–Menten kinetics (CN^- and (*S*)-**1** as substrates) with competitive inhibitions by (*R*)-**1** and DMSO (eq 4). Both kinetic models for biocatalytic reactions include operational stability decay rate constants (k_d). The constants were estimated from independent activity measurements in batch reactors (Figure S7, Table S2, SI). The mass-balance equations describing the change in the concentration of the reaction compounds in the batch reactor are given (Table 1, eqs 6–11). The operational stability decay is described by the first-order kinetics (Table 1, eq 12), while the dependence of k_d on the initial concentration of *rac*-**1** is described by a hyperbolic function (Table 1, eq 13).

2.8. Whole-Cell Immobilization and the Scale-Up Reaction. *2.8.1. Immobilization in Alginate Beads.* Immobilization of whole cells was performed according to a slightly modified standard procedure.[37] Upon cell harvesting (see Section 2.2), *E. coli* cells harboring the ISM-4 enzyme were frozen at −70 °C and subsequently lyophilized (p = 0.028 mbar, T = −46 °C, FreeZone, Labconco, USA). After lyophilization, cell entrapment in alginate beads was performed. Dry cells (240 mg) were added to a 2% w/v sodium alginate solution in acetate buffer (pH 5.5). Following homogenization for 15 min, a solution of 100 mM calcium lactate was added dropwise with a buret to the cell suspension, forming 2 mm spherical alginate beads with entrapped *E. coli* cells. After curing for 1 h, the beads were washed in ultrapure water and immediately used for the scale-up experiment.

2.8.2. Scale-Up Reaction. The scale-up reaction was performed in a rotating-bed reactor (RBR, AB SpinChem, Sweden) with alginate beads entrapping whole *E. coli* cells. Upon loading the beads into a separate compartment, 100 mL

https://doi.org/10.1021/acs.iecr.4c00477
Ind. Eng. Chem. Res. 2024, 63, 7051−7063

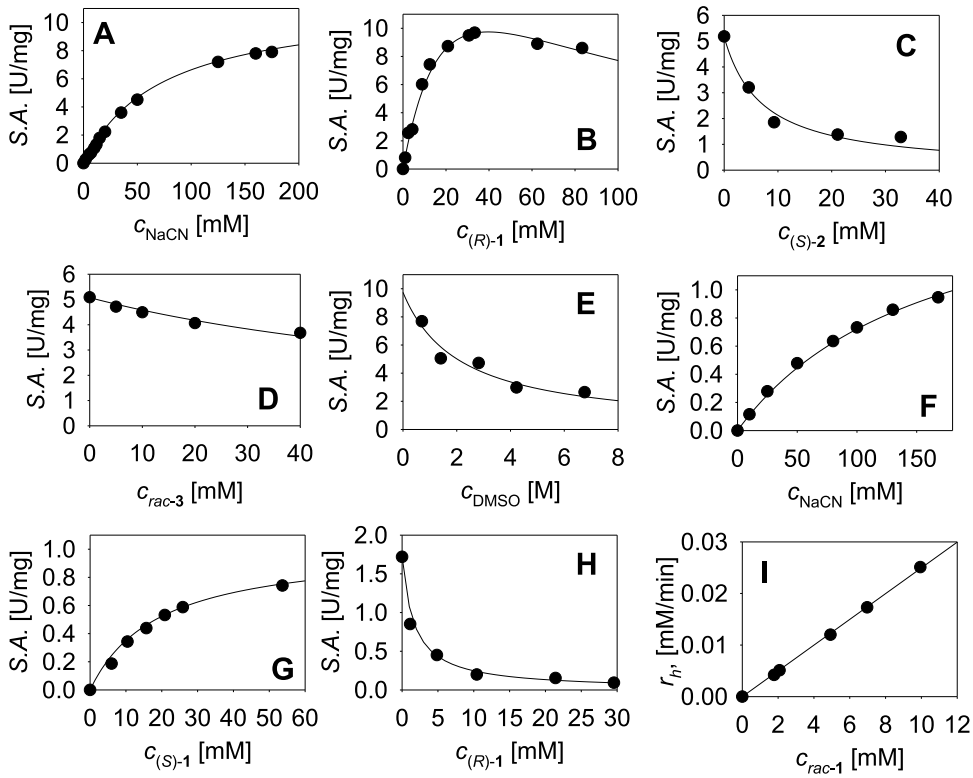

Figure 1. Kinetics of the kinetic resolution of *rac*-**1** in the presence of cyanide ions and the ISM-4 enzyme (V_r = 500 μL; 500 mM Tris−SO_4; pH 7.5; 25 °C; DMSO 10% v/v; 1000 rpm). Graphs A−E correspond to the scheme given in Scheme S2A (SI), which is biocatalytic synthesis of (*S*)-**2** from (*R*)-**1**; graphs F−H correspond to the scheme given in Scheme S2B (SI), which is biocatalytic synthesis of (*R*)-**2** from (*S*)-**1**; and graph **I** corresponds to the scheme given in Scheme S2C (SI), which is spontaneous hydrolysis of *rac*-**1**. Black dots—experimental data and line—mathematical model.

of a reaction mixture was prepared by adding DMSO (10 mL, 10% v/v), *rac*-**1** (0.69 g, 50 mM), and NaCN (0.25 g, 50 mM) to 90 mL of Tris−SO_4 buffer (500 mM, pH 7.5). Synthesis was performed at 25 °C and 600 rpm, and samples were processed in the same manner as described previously (see Section 2.3).

3. RESULTS AND DISCUSSION

3.1. Enzyme Kinetics. The observed reaction system (Scheme 1) can, in fact, be divided into three individual reactions (Scheme S2, SI). The first is the biocatalytic conversion of (*R*)-**1** to (*S*)-**2** (Scheme S2A, SI), where the relative configurations of the substrate and the product are the same, but an inversion of the absolute configuration occurs due to different substituent priority according to the Cahn−Ingold−Prelog rule. The second reaction is the biocatalytic conversion of (*S*)-**1** to (*R*)-**2** (Scheme S2B, SI), while the third is the chemical hydrolysis where *rac*-**3** is produced (Scheme S2C, SI). A chemical reaction between *rac*-**1** and NaCN and biocatalytic hydrolysis of *rac*-**1** were screened for but not detected. Kinetic characterization was performed for both biocatalytic reactions (Scheme S2A,B, SI) and spontaneous hydrolysis (Scheme S2C, SI). The apparent kinetic parameters (Table S1, SI) were estimated based on the reaction schemes (Scheme S2A−C) and the experimental data (Figure 1) obtained by the initial reaction rate method. More information regarding kinetic models used for estimation of each kinetic parameter is given in the Supporting Information (Table S1, SI). The synthesis of (*S*)-**2** is described by the double-substrate Michaelis−Menten kinetics with substrate inhibition by (*R*)-**1** and inhibitions by (*S*)-**2**, *rac*-**3**, and cosolvent DMSO. Likewise, the synthesis of (*R*)-**2** is described by double-substrate Michaelis−Menten kinetics with inhibitions by cosolvent DMSO and the opposite enantiomer of the substrate, (*R*)-**1**. The hydrolytic reaction is an inevitable side reaction described by pseudo-first-order kinetics. This means that hydrolysis is a bimolecular reaction in which a water molecule and an epoxide molecule react, but water is present in large excess and can therefore be considered mathematically as a part of the constant (k_h).

Determination of the kinetic parameters confirmed the enantiopreference of the ISM-4 enzyme in the synthesis of (*S*)-**2** compared to (*R*)-**2** since the apparent maximum reaction rate is 10-fold higher (Table S1, SI, V_{m1} = 42.211 U/mg; V_{m2} = 4.994 U/mg). Furthermore, in the synthesis of (*S*)-**2**, the enzyme displays higher affinity toward cyanide ions since the apparent Michaelis constant is approximately 3-fold lower (Table S1, SI, K_{m1}^{CN} = 67.735 mM; K_{m2}^{CN} = 194.581 mM), whereas the apparent Michaelis constants for epoxides are roughly comparable (Table S1, SI, $K_{m1}^{(R)-1}$ = 26.704 mM; $K_{m2}^{(S)-1}$ = 19.049 mM). Although the synthesis of (*S*)-**2** is by far more favored compared to the synthesis of (*R*)-**2**, there are different inhibitions to be considered. The presence of DMSO mildly affects both reactions equally through mixed inhibition properties with a predominant competitive share (Table S1, SI, K_i^{DMSO} = 1546.7 mM).[34] The synthesis of (*S*)-**2** is also inhibited by substrate (*R*)-**1** concentrations higher than 50 mM. Additionally, the synthesis of (*S*)-**2** is highly influenced by the concentration of the forming biocatalytic product (Table S1, SI, $K_{i1}^{(S)-2}$ = 5.109 mM) and to a lesser extent by the hydrolytic product, *rac*-**3** (Table S1, SI, K_i^{rac-3} = 73.94

https://doi.org/10.1021/acs.iecr.4c00477
Ind. Eng. Chem. Res. 2024, 63, 7051−7063

mM). On the other hand, the synthesis of (*R*)-**2** is negatively affected by the presence of (*R*)-**1** (Table S1, SI, $K_{i2}^{(R)-1}$ = 1.102 mM).

The inhibition of ISM-4 by *rac*-**3**, which is present in the synthesis of (*S*)-**2** and not in the synthesis of (*R*)-**2**, clearly shows how the kinetic profiles obtained by investigating one enantiomer do not always correlate with the situation present with the other.[38] It is worth highlighting that such a selective inhibition of the enzyme only in the reaction with one enantiomer could be due to several factors. These include, but are not limited to, steric hindrance, differences in stereochemistry and conformational preferences, and interference of inhibitors with specific steps in different reaction pathways with two enantiomers. For instance, *rac*-**3** may interact more effectively with the active site when the preferred (*R*)-enantiomer of the substrate is bound, leading to steric hindrance and inhibition. As the active site of the enzyme has higher specificity for the (*R*)-enantiomer of the substrate, it could make it more susceptible to inhibition by the diol, while the inhibition of the enzyme in the reaction with the (*S*)-enantiomer could also occur but in the concentrations higher than ones investigated in this study. Another possible explanation could be that *rac*-**3** is not strictly affecting the active site, but its binding to the enzyme may induce such conformational changes that enhance its inhibitory effect on the biocatalytic reaction with (*R*)-**1**, while having little to no effect on the reaction with opposite enantiomer. All of the other interdependencies that are not listed, e.g., the effect of *rac*-**3** on the synthesis of the (*R*)-**2**, were tested but had no effect on the specific activity. The hydrolytic reaction is described by first-order kinetics with a hydrolysis constant of 0.0025 min^{-1}, which means that increasing the concentration of *rac*-**1** leads to the formation of *rac*-**3** to a greater extent. Further explanations of the kinetic results and their implication for the synthesis outcomes can be found later (see Sections 3.3. and 3.4).

Such knowledge of the kinetic behavior of HHDH-catalyzed systems represents valuable information since kinetic constants are rarely found for this enzyme family in the literature. In 2020, in our research group,[14] we have reported that fundamental kinetic constants (K_m, k_{cat}) are usually only given within the initial screening of enzyme activities toward substrates or nucleophiles[39−41] or as a mean of comparison of the performance of wild-type enzymes and their mutants.[29,42] Out of approximately 100 existing scientific papers dealing with some aspect of HHDH-catalyzed reactions, only 7 of them reported the presence of enzyme inhibitions.[14] Since in the current research, we have shown that this enzyme is inhibited by the substrate, product, byproduct, and solvent (Figure 1), we could assume that it is highly improbable that inhibitions are not present in other investigated systems. In most of the analyzed studies with HHDHs reported up to now, enzyme inhibitions may have gone unnoticed because the concentrations of substrates were too low (1−5 mM) for such phenomena to be observed or determined with certainty.

A detailed kinetic study on HHDH enzymes has been published recently in our group,[35] focusing on the characterization of biocatalytic azidolysis of 2-[4-(trifluoromethyl)-phenyl]oxirane proceeding with complete enantioselectivity. Despite the differences between the investigated biocatalytic systems in the substrate structure (different fluorinated aromatic epoxides), nucleophile (azide and cyanide ions), enzyme variants (W249P and ISM-4), and side reactions present in the investigated systems, similarities in the kinetic observations between cited[35] and current research have been observed, especially when it comes to enzyme inhibitions. For example, epoxides act as inhibitors in both biocatalytic reactions. Moreover, inhibitions by the opposite enantiomers of the substrate, the formed biocatalytic product, the byproduct diol, and the cosolvent DMSO are present as well,[35] whereby the latter was also confirmed in other investigated HHDH-catalyzed reactions.[34] In our first studies regarding HHDH-catalyzed transformations of fluorinated styrene oxide derivatives, we have found that cyanolysis reactions, despite representing a high potential for the synthesis of optically pure valuable compounds, proceed with reduced efficiency on a higher concentration scale.[30] To scale up completely enantioselective cyanolysis of 2-[4-(trifluoromethyl)phenyl]oxirane with HheC-W249P, high enzyme loadings were required, along with extended reaction times, to achieve only a 30% yield. Considering our current understanding of the kinetics in an analogous system, we could assume that the elevated enzyme concentrations were required so the synthesis could be carried out despite the presence of inhibitions, and the final yield was significantly reduced due to the hydrolytic effect, which is particularly pronounced at higher substrate concentrations. Additional similarities among HHDH-catalyzed systems are elaborated and commented on in the sections below.

3.2. Stability of the Enzyme during Incubation with an Epoxide and a Nucleophile. Except by inhibitions, the reaction outcome can be negatively affected by the stability of the enzyme. The loss of enzyme activity can be affected by numerous external influences, including time and the composition of the reaction mixture. Hence, ISM-4 stability was evaluated during time in a buffer medium and in the presence of various epoxide and nucleophile concentrations. Stability measurements during incubation with substrates were performed over 3 days due to high enzyme stability at resting conditions. When monitoring enzymes of high stability, measurements need to be performed over a longer period in order to detect a definite and clear change in activity. The effect of both *rac*-**1** and CN^- on enzyme stability was tested, but measurements were performed in the presence of one compound at the time to prevent the reaction between them. The results revealed that the concentration of sodium cyanide does not have any influence on ISM-4 stability, as the trend of deactivation is the same in the case of all concentrations of the nucleophile as without it (Figure 2A). On the other hand, in the presence of higher *rac*-**1** concentrations, the deactivation was more severe, whereby the highest deactivation rate was recorded at the highest epoxide concentration (Figure 2B).

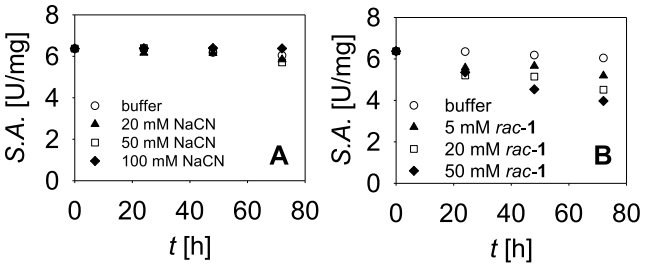

Figure 2. Influence of (A) NaCN and (B) *rac*-**1** on stability of ISM-4 during incubation (500 mM Tris−SO_4 pH 7.5, 25 °C, 1000 rpm, V_r = 0.5 mL, γ_{ISM-4} = 1 mg/mL).

https://doi.org/10.1021/acs.iecr.4c00477
Ind. Eng. Chem. Res. 2024, 63, 7051−7063

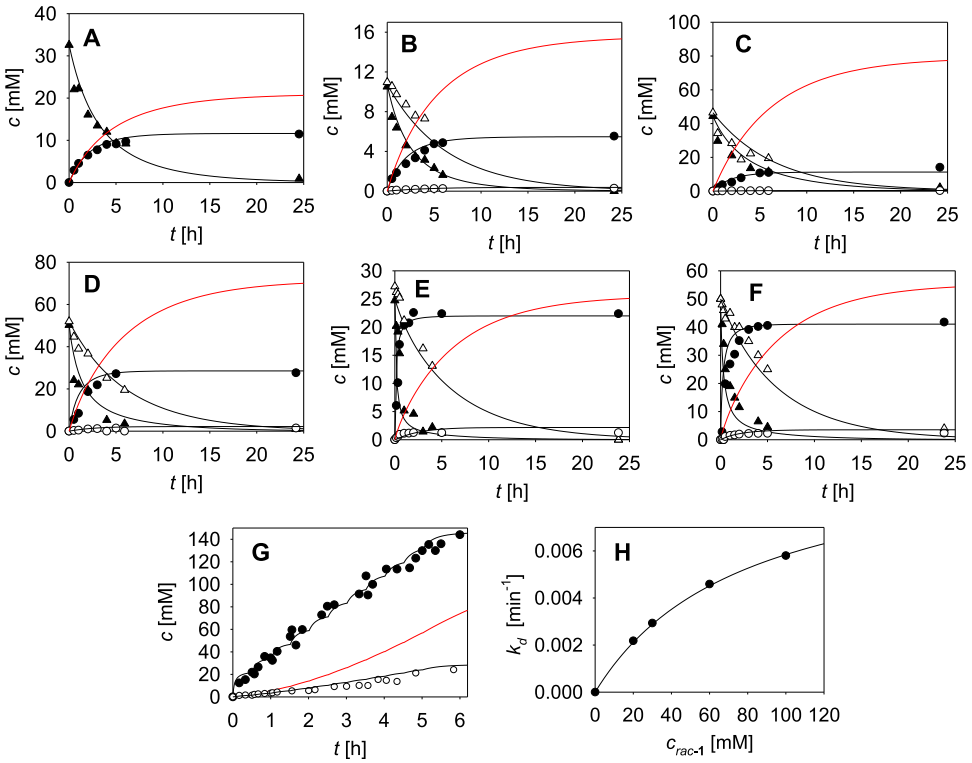

Figure 3. Model validation in the batch reactor (c_{DMSO} = 1.4 M): (A) $c_{(R)\text{-}1}$ = 33 mM, c_{NaCN} = 150 mM, and $\gamma_{ISM\text{-}4}$ = 0.01 mg/mL; (B) $c_{rac\text{-}1}$ = 21.5 mM, c_{NaCN} = 150 mM, and $\gamma_{ISM\text{-}4}$ = 0.01 mg/mL; (C) $c_{rac\text{-}1}$ = 91 mM, c_{NaCN} = 150 mM, and $\gamma_{ISM\text{-}4}$ = 0.01 mg/mL; (D) $c_{rac\text{-}1}$ = 102 mM, c_{NaCN} = 150 mM, and $\gamma_{ISM\text{-}4}$ = 0.05 mg/mL; (E) $c_{rac\text{-}1}$ = 52 mM, c_{NaCN} = 25 mM, and $\gamma_{ISM\text{-}4}$ = 1 mg/mL; and (F) $c_{rac\text{-}1}$ = 100 mM, c_{NaCN} = 50 mM, and $\gamma_{ISM\text{-}4}$ = 0.5 mg/mL. (G) Repetitive-batch reactor ($c_{rac\text{-}1}$ = 100 mM, c_{NaCN} = 50 mM, $\gamma_{ISM\text{-}4}$ = 0.5 mg/mL) with addition of 50 mM *rac*-**1** and 25 mM NaCN every 30 min to 5 h. Legends (A–G) experimental data—symbols, simulations—lines. ▲ (*R*)-**1**, Δ (*S*)-**1**, ● (*S*)-**2**, ○ (*R*)-**2**, and (red—full line) *rac*-**3**. (H) Dependency of k_d^{ISM-4} on the $c_{rac\text{-}1}$ in the batch reactor.

This data trend insinuates that epoxide amount could have an important role in enzyme operational stability as well.[35,43,44] Such behavior could be due to esterification of protein carboxyl groups or nonspecific chemical reactions between epoxide rings and protein functional groups of a nucleophilic character, such as amino-, hydroxyl-, or thiol- groups, leading to random alterations on the protein surface.[45,46]

3.3. Model Validation. To confirm the validity of the developed mathematical model, a series of batch reaction experiments were performed with different initial concentrations of substrates and enzymes (Figure 3A–F). Besides determining the concentrations of the reaction compounds, the validation included the monitoring of the operational stability of the ISM-4 variant by performing a series of individual enzyme activity measurements through the reaction time (Figure S7, Table S2). Operational stability decay rate constants (k_d) were estimated from the decline in enzymatic activity and were integrated into the developed mathematical model (Table 1, eqs 3 and 4). The mathematical model has proven to fit the experimental data well (Table S3), and as such, it can be used to describe and simulate different outcomes of the studied process. During model validation, the enantiomeric ratio (E = 28) of the enzyme was calculated from the values of enzymatic conversion and optical purities of the substrate and the product. As the E-value in the range of 15–30 is considered moderate to good, while values above 30 are considered excellent,[47] ISM-4 was further evaluated as a favorable candidate for the respective synthesis, with a special emphasis on the effect of different reaction conditions on the reaction outcome. At very low enzyme concentrations (Figure 3A–D; 0.01–0.05 mg/mL CFE), the biocatalytic reactions are rather slow, and high concentrations of *rac*-**3** are formed (represented only by red lines based on mathematical model simulations due to weak response in analytical methods applied). When the enzyme loadings are sufficient (Figure 3E,F; 0.5 and 1 mg/mL CFE), the biocatalytic transformation of (*R*)-**1** to (*S*)-**2** occurs rapidly. In this case, if the reaction is not terminated at the time of complete (*R*)-**1** consumption, the conversion of (*S*)-**1** continues in the biocatalytic and hydrolytic reaction, with serious implications for both the yield and optical purity of the desired compounds (Table 2). For example, in the experiment depicted in Figure 3E, prolongation in the reaction time results in the drop in cyanohydrin (*S*)-**2** selectivity from 3.5 to 0.8, and the epoxide (*S*)-**1** yield from 81.8 to 2.4%. Here, the yield is defined as the ratio of the quantity of the obtained product over the

Table 2. Values of Process Metric s (Yield, Selectivity, and Optical Purity) in Batch Experiments Depending on the Duration of the Biocatalytic Reaction[a]

	exp. E				
	$Y_{(S)\text{-}2}$, %	$S_{(S)\text{-}2}$, /	$Y_{(S)\text{-}1}$, %	ee_s, %	ee_p, %
1 h	80.6	3.5	81.8	70	90
24 h	88.0	0.8	2.37	86	82
exp. F					
1 h	70.2	3.1	83.6	57	93
24 h	82.1	0.7	2.44	80	85

[a]Process metrics are defined in eqs S7–S9 (SI).

https://doi.org/10.1021/acs.iecr.4c00477
Ind. Eng. Chem. Res. 2024, 63, 7051–7063

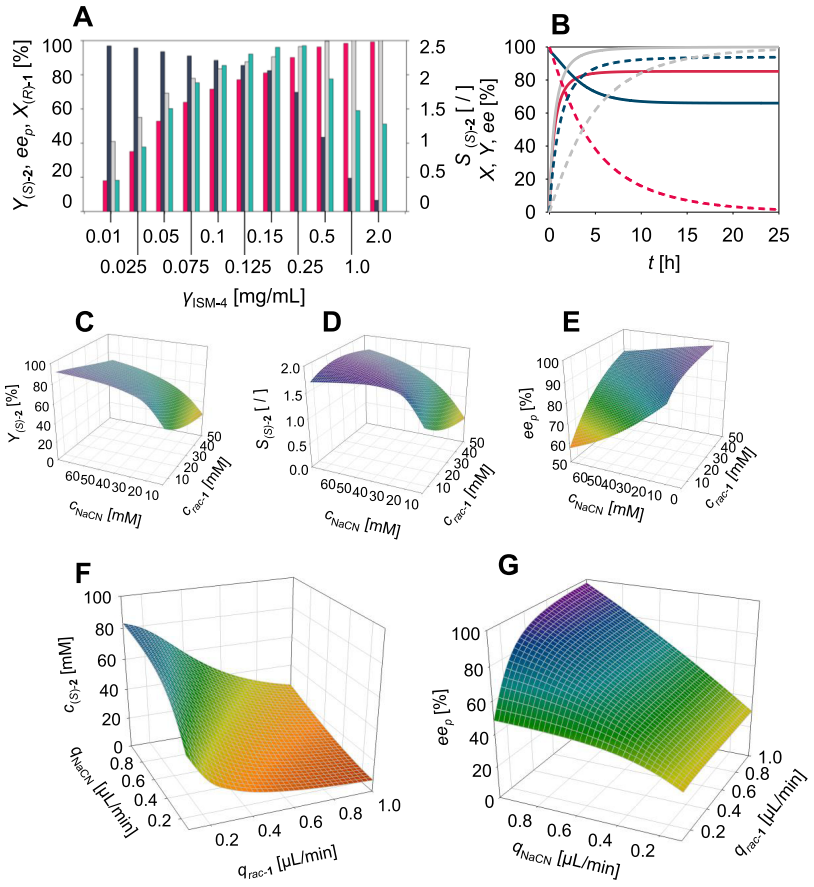

Figure 4. Batch reactor (A–E): dependency of (A) $Y_{(S)\text{-}2}$ (red solid box), ee_p (blue solid box), $X_{(R)\text{-}1}$ (gray solid box), and $S_{(S)\text{-}2}$ (cyan solid box) on $\gamma_{ISM\text{-}4}$ (c_{DMSO} = 1.4 M, $c_{rac\text{-}1}$ = 50 mM, c_{NaCN} = 75 mM, 2 h); (B) $Y_{(S)\text{-}2}$ (red dash), ee_p (blue dash), and $X_{(R)\text{-}1}$ (gray dash) on reaction time (solid line $Y_{(S)\text{-}2}$, ee_p, $X_{(R)\text{-}1}$; dashed line $Y_{(S)\text{-}1}$, ee_s, $X_{(S)\text{-}1}$) (c_{DMSO} = 1.4 M, $c_{rac\text{-}1}$ = 50 mM, c_{NaCN} = 75 mM, $\gamma_{ISM\text{-}4}$ = 0.125 mg/mL); and (C) $Y_{(S)\text{-}2}$, (D) $S_{(S)\text{-}2}$, and (E) ee_p on employed *rac*-**1** and CN^- concentrations (c_{DMSO} = 1.4 M, $\gamma_{ISM\text{-}4}$ = 0.125 mg/mL, 2 h). Fed-batch reactor (F–G): dependency of (F) $Y_{(S)\text{-}2}$ and (G) ee_p on employed *rac*-**1** and CN^- flow rates ($q_{rac\text{-}1}$, q_{NaCN}) ($V_{r,0}$ = 10 mL, $c_{0,rac\text{-}1}$ = 50 mM, $c_{0,NaCN}$ = 25 mM, $\gamma_{ISM\text{-}4}$ = 1 mg/mL, 6 h. Stock solutions in pistons calculated as maximum theoretical values; $c_{rac\text{-}1,piston}$ = 7.8 M, $c_{NaCN,piston}$ = 12.9 M).

theoretically possible maximum product quantity, whereas selectivity is the ratio of the quantity of the obtained desired products over the quantity of the obtained undesired product, in this case, both (*R*)-**2** and *rac*-**3**. When the reaction is performed in repetitive mode (Figure 3G), which implies the periodic addition of a new portion of *rac*-**1** to the reactor per consumption of (*R*)-**1**, the formation of (*R*)-**2** and *rac*-**3** can be controlled and lowered, since the reacting substrates are kept constantly at low concentrations. In this case, high product concentration is obtained ($c_{(S)\text{-}2}$ = 145 mM), with moderate optical purity (ee_p = 80%). The improvement in the process metrics in the repetitive-batch reactor compared to the standard batch reactor is a result of several factors. First is the minimization of the enzyme inhibition by (*S*)-**1**. The second factor involves the minimization of enzyme deactivation, which is more pronounced at a higher *rac*-**1** concentration. Third is diol formation, as in the hydrolysis reaction, not only (*R*)-**1** is spent but also formed *rac*-**3** inhibits the enzyme activity. The implications of the reaction outcome of different initial conditions and the distribution of substrate dosage over time in the reactor, together with the importance of controlling the reaction time, will be discussed in more detail later.

As already implied by enzyme incubation studies, the enzyme operational stability study revealed that the estimated k_d values increase with higher initial concentrations of *rac*-**1** in the reactor (Figure S7, Table S2); moreover, a regular hyperbolic trend of dependence was observed (Figure 3H).[35,43,44] The empirical equation describing the dependence of k_d on *rac*-**1** concentration is given in Table 1, eq 13, and the respective parameters (a, b) are listed in Table S1 (SI). The trend of enzyme deactivation with increasing epoxide concentration might be attributed to the nonspecific intramolecular interactions between epoxide rings and nucleophilic functional groups on the enzyme surface, as discussed earlier (see Section 3.2). The enzyme deactivation was described and numerically included in the mathematical model, but the actual mechanism of enzyme deactivation in the presence of epoxide was not further investigated.

A handful of enzymes are stable when exposed to small organic molecules only on a millimolar scale that corresponds to the concentrations found in a physiological environment. Higher substrate loadings, usually required for economically profitable synthesis, may lead to irreversible changes in the protein native structure and, consequently, enzyme deactivation. Thus, enzyme tolerance toward higher substrate concentrations is an important parameter when evaluating enzymes as catalysts for synthetic procedures. However, there are very limited data in the existing literature on HHDHs' operational stability and the influences of different process parameters on the stability decay. Similar to enzyme inhibitions that may have gone unnoticed due to too low

https://doi.org/10.1021/acs.iecr.4c00477
Ind. Eng. Chem. Res. 2024, 63, 7051−7063

concentrations of substrates employed in respective studies, as already discussed, concentration-dependent operational stability decay cannot be detected during activity screening at substrate concentrations of 1−5 mM without repeating experiments with the same enzyme loadings. A hyperbolic dependence of HheC-W249P operational stability decreasing with increasing 2-[4-(trifluoromethyl)phenyl]oxirane concentration was only found within our previous research,[35] suggesting that the HheC enzyme variants are deactivated in the presence of higher concentrations of fluorinated aromatic epoxides.

3.4. Process Enhancement through Model-Based Simulations. Although enzymes can exhibit high potential in terms of activity and enantioselectivity at a low concentration scale, the presence of different inhibitions, deactivation, and chemical reactions significantly affects the outcome at elevated substrate concentrations. Therefore, model-based simulations are a powerful tool for the prediction of the reaction outcome and optimization of process conditions, especially on a higher concentration scale. Increasing the enzyme concentration within reasonable limits in order to favor the biocatalytic reaction and decrease the diol formation is a logical step that does not seem to require an understanding of the entire mathematical model, as the effect of hydrolysis can be almost completely avoided by using sufficiently high enzyme loadings. For instance, based on the guidelines and cost analysis for biocatalytic syntheses, it is recommended to utilize up to 1 g of free enzyme for the synthesis of 67−170 g of the product.[48] However, the enzyme is often the most expensive compound when the profitability of the process is considered, so model-based simulations can be used for the determination of the optimal enzyme amount needed for completion of the studied reaction without unnecessary and expensive overconsumption. Moreover, as already briefly discussed in the previous section, the situation is even more complicated when an enzyme catalyzes both the main and the side reactions. This is the case for (*R*)-**1** and (*S*)-**1** conversion, where increasing the enzyme concentration accelerates both the desired and undesired biocatalytic reaction. Figure 4A displays the change in the yield of the targeted product ($Y_{(S)\text{-}2}$), substrate conversion ($X_{(R)\text{-}1}$), product enantiomeric excess (ee_p), and reaction selectivity ($S_{(S)\text{-}2}$) with varying the amount of the employed enzyme. At lower CFE concentrations, the optical purity of the product is close to the theoretical maximum, while at the other end of the investigated scale, both the product yield and substrate conversion reach nearly 100%. However, in both concentration extremes (0.01 and 2.0 mg/mL CFE), the maximum values of some performance indicators come at the expense of the others. In the 0.1−0.25 mg/mL range, this is not the case. For example, at 0.125 mg/mL CFE, substrate (*R*)-**1** conversion and the resulting (*S*)-**2** product yield exceed 80%, with ee_p 90% and selectivity 2. These simulations demonstrate how only good knowledge of the mathematical model can lead to the correct selection of the exact enzyme amount that should be employed.

Where the mathematical model also comes in quite handy is the manipulation of variables, whose influence on the reaction outcome is not so obvious. As the cyanolysis of *rac*-**1** is a kinetic resolution, the reaction outcome should be evaluated in a time-wise manner as well. In the reactions of kinetic resolutions, it is necessary to terminate the reaction at the latest after achieving full conversion of the desired enantiomer of the substrate. Depending on the enantioselectivity of the enzyme employed, it may be necessary to terminate the reaction even earlier in order to obtain the desired product of high optical purity. Figure 4B presents the course of the same reaction (c_{DMSO} = 1.4 M, $c_{rac\text{-}1}$ = 50 mM, c_{NaCN} = 75 mM, $\gamma_{ISM\text{-}4}$ = 0.125 mg/mL) through time. The reaction should be terminated immediately after the consumption of (*R*)-**1**, as further contact of (*S*)-**1** with the reaction compounds leads to its conversion to (*R*)-**2** and *rac*-**3**. Figure 4B demonstrates that, under given conditions, prolongation of the reaction after 2 h leads both to the reduction of enantiomeric excess of (*S*)-**2** and yield of (*S*)-**1**. Since terminating the kinetic resolution reactions on time plays a key role in the quality of final products, this example serves as a practical illustration of the value of model-based simulations, particularly when real-time concentration monitoring is not an option.

Sodium cyanide is a nucleophile in both biocatalytic reactions; therefore, it is expected to have an influence on the yield and the optical purity of the product. When performing HHDH-catalyzed reactions, the nucleophile salt is usually added in 1.5−2 mol equiv respective to the epoxide.[16,30,49−52] Further simulations were performed with variations of *rac*-**1** (5−50 mM) and cyanide concentration (10−75 mM), whereby optical purity, product yield, and selectivity were observed (Figure 4C−E). Although (*S*)-**2** yield and selectivity are satisfactory at high cyanide and low epoxide concentrations (95% and 1.7, respectively), the optical purity of the resulting product is inadequate under the same conditions. Observing simultaneously all three performance indicators, it is obvious that, in this case, the best overall results can be obtained by initiating reactions with *rac*-**1** and NaCN concentrations around 30 and 40 mM, respectively.

Substrate concentrations have a great influence on the reaction outcome, and as such, they should be carefully selected and monitored. Since (*S*)-**2** synthesis is inhibited by substrate (*R*)-**1**, and cyanide ions participate both in desired and undesired biocatalytic reactions, a fed-batch reactor is an option worth considering, as it offers improved control over substrate distribution throughout the whole reaction time, rather than just initial concentrations adjustment, as is the case with the batch reactor. Figure 4F,G displays how a range of NaCN and *rac*-**1** flow rates influences the concentration and optical purity of the desired product, (*S*)-**2**. As depicted in Figure 4F,G, by distributing substrate loading in a reactor through time, quite different scenarios can be obtained. For example, adjusting both flow rates at 1 μL/min provides around 100 mM product (*S*)-**2** but with very low optical purity ($ee_p \approx 30\%$). This occurs due to overloading of the substrate, (*R*)-**1**, which displays inhibition above 25 mM and accumulation of inhibiting product (*S*)-**2** and byproduct *rac*-**3**. However, by lowering the *rac*-**1** flow rate to 0.35 μL/min and keeping NaCN at 1 μL/min, a highly improved scenario is achieved ($c_{(S)\text{-}2}$ > 75 mM, ee_p > 90%).

3.5. Scale-Up Reaction. To further assess the potential of the studied biocatalytic synthesis, the reaction was carried out on a preparative scale (100 mL). Instead of the isolated enzyme, whole cells of *E. coli* expressing the ISM-4 enzyme were used and immobilized in calcium alginate beads (Figure S8A, SI). This approach was chosen to simulate conditions more acceptable for industrial synthesis, as whole-cell immobilization reduces the cost of biocatalyst preparation and opens the possibility of its recovery and reuse. The reaction was carried out in RBR (SpinChem AB, Sweden)

https://doi.org/10.1021/acs.iecr.4c00477
Ind. Eng. Chem. Res. 2024, 63, 7051−7063

(Figure S8B, SI). RBR was selected since this technology ensures more efficient mass transfer while minimizing the possibility of soft bead damage by avoiding the usage of classic stirred vessels.[53] The initial conditions, i.e., concentrations for the scale-up reaction, were chosen based on findings from the mathematical model for the free enzyme (50 mM *rac*-**1**, 50 mM NaCN, 10% DMSO v/v). However, it should be emphasized that there are some fundamental differences between the different forms of biocatalysts, i.e., isolated enzymes and whole cells, which can significantly affect reaction kinetics and performance. For example, enzyme activity and stability may be affected by the presence of other compounds in the complex intracellular environments. Additionally, mass transfer limitations and substrate accessibility within the whole cells can have a great influence on reaction kinetics. Although it is expected that the kinetic parameters will somewhat change with different forms of biocatalysts (isolated enzyme vs whole cells, free enzyme vs immobilized), the model can serve as a good foundation for the selection of reactor configuration and initial conditions for avoiding biotransformation bottlenecks.[54,55] For instance, inhibitions and concentration-dependent deactivations that were discovered for the free enzyme are likely to be present within whole cells as well, although their extent may vary. At a 100 mL scale, the reaction was carried out starting from 50 mM *rac*-**1** and 50 mM NaCN and was terminated after 6.5 h. The time point for the termination of the synthesis was selected based on monitoring of product concentration over time in the respective experiment, but also with the judgment based on knowledge from the mathematical model and validation experiments. Since between 4 and 6.5 h the concentration of the product did not increase considerably (Figure S9, SI), and meanwhile, the concentration of the substrate continued to decrease, it was concluded that further contact of the unreacted substrate with the reaction mixture would lead to the reduction of the (*S*)-**1** yield. The reaction resulted in 24.7 mM **2** ($Y_{(S)\text{-}2}$ = 71.6%, ee_p 92%) and 20.2 mM **1** ($Y_{(S)\text{-}1}$ = 68.1%, ee_s 87.6%) (Figure S9, SI), while the remaining 5.1 mM missing in the balance was attributed to the formation of a diol. On the account of measured concentrations of the products of interest, together with calculated yields and ee values, we believe that this process holds a valuable synthetic potential that should further be investigated. However, to meet the rigorous criteria of the pharmaceutical industry, ee_p values should be greater than 99%, a threshold that can be obtained by ISM-4 only at lower substrate concentrations, consequently resulting in lower final product concentrations. Based on these results and kinetic insights from the presented study, including enzyme deactivation and intensification of unwanted reactions at a higher concentration scale, more research is needed on possible immobilization techniques, including the alginate entrapment demonstrated here. The stability of such biocatalyst forms in different media throughout the prolonged period should be evaluated, with the aim of transitioning toward continuous processes, where substrate concentrations could theoretically be maintained at levels that would result in the product of satisfactory optical purity.

4. CONCLUSIONS

In this research, the biocatalytic synthesis of an enantioenriched fluorinated cyanohydrin was studied by the reaction engineering approach. During kinetic characterization, inhibitions by the substrate (*R*)-**1**, the product (*S*)-**2**, the byproduct *rac*-**3**, and the solvent DMSO were detected, together with the substrate-dependent enzyme deactivation. These observations were correlated with the previously obtained kinetic data from another HHDH-catalyzed system employing a different set of enzyme variants, substrates, and nucleophiles, leading to a better overall understanding of the kinetic behavior of such systems. Since, in the observed system, the enantioselectivity of the enzyme toward (*R*)-**1** is not absolute, the optical purity of the final products is not guaranteed under all experimental conditions. Through process simulations based on a thoroughly developed mathematical model incorporating the effects of both enzyme-catalyzed reactions as well as hydrolytic degradation, reaction bottlenecks were addressed, and their effect on the process outcome was minimized. Careful selection of substrate and enzyme concentration, control of reaction time, and distribution of substrate dosage over time provided great improvement compared to the first (*S*)-3-(4-fluorophenyl)-3-hydroxypropanenitrile synthesis attempts in a batch reactor. Substrate dosing in the fed-batch and the repetitive-batch reactor resulted in the 75 and 145 mM desired product with ee > 90 and 80%, respectively. The applicability of this synthesis was also demonstrated on higher scale, where immobilized whole cells harboring the ISM-4 enzyme were employed in successful synthesis on a 100 mL scale. The reaction conditions for the scale-up synthesis were selected based on the mathematical model simulations, yielding the 24.7 mM product (Y = 72%, ee 92%). With this research, we have shown that with a deep understanding of the biocatalytic system aided by the mathematical model and manipulation of the reaction conditions through process simulations, it is possible to obtain products of high optical purity and high yield, all within the limits of the enzyme. The findings from the developed model for the free enzyme can serve not only as a basis for the understanding of the processes catalyzed by the ISM-4 enzyme in various forms (whole-cell biocatalyst, immobilized biocatalyst) but also as a valuable framework for expanding the applicative scope of HHDH enzymes. This is particularly appropriate for the synthesis of optically pure or enantioenriched products using HHDH enzymes with incomplete enantioselectivity. Additionally, the mathematical model proves beneficial for syntheses starting from hydrolytically unstable substrates prone to decomposition in the reaction medium. Furthermore, the model increases our understanding of the underlying factors contributing to poor performance when attempting to increase the working concentration range, thereby offering guidance to researchers in selecting suitable reactor types and initial conditions. Through this research, several bottlenecks affecting the synthetic potential of the ISM-4 enzyme have been identified, including enzyme inhibitions, substrate-dependent deactivation, and the pronounced hydrolysis effect. Future efforts should prioritize investigating additional enzyme immobilization techniques and reaction media engineering. Stabilizing the biocatalyst and transitioning to alternative media are steps toward switching to continuous mode. Such an approach could be beneficial for the reduction of the hydrolysis effect, inhibitions, and enzyme deactivation, thereby enhancing the efficiency and scalability of the respective biocatalytic process.

■ ASSOCIATED CONTENT

Supporting Information

The Supporting Information is available free of charge at https://pubs.acs.org/doi/10.1021/acs.iecr.4c00477.

https://doi.org/10.1021/acs.iecr.4c00477
Ind. Eng. Chem. Res. 2024, 63, 7051−7063

(SI 1) Synthetic procedures for (*S*)-4-fluorostyrene oxide and (*R*)-3-(4-fluorophenyl)-3-hydroxypropanenitrile (Protocol S1); (SI 2) reaction scheme of the ring closure of *para*-nitro-2-bromo-1-phenylethanol (PNSHH) to *para*-nitro styrene oxide (PNSO) catalyzed by HHDH used as activity assay in the respective study (Scheme S1); (SI 3) SDS-PAGE of the ISM-4 variant employed in the respective study (Figure S1); (SI 4) chromatograms and calibration curves for HPLC and GC analyses (Figures S2−S5); (SI 5) reaction schemes of all of the reactions included in the observed biocatalytic system (Scheme S2); (SI 6) estimated kinetic parameters for the reactions occurring in the investigated reaction system (Table S1); explanation of the kinetic models used for estimation of kinetic parameters (equations S1−S2); and parity plots depicting experimental vs predicted specific activities (Figure S6); (SI 7) enzyme operational stability data including graphical representation of operational stability decay during batch experiments and estimated stability decay rate constants (Figure S7, Table S2); (SI 8) statistics on fitting of model simulations and experimental data collected during model validation experiments in the batch reactor (Table S3) and explanation of goodness-of-fit statistics (standard deviations, coefficients of determination, correlation coefficients, model selection criterions) (equations S3−S6); (SI 9) definitions of parameters used to characterize the extent of a desired reaction over side reactions (yield, selectivity, enantiomeric excess) (equations S7−S9); and (SI 10) additional information on the scale-up reaction in the RBR reactor employing alginate beads with immobilized cells (Figures S8 and S9) (PDF)

AUTHOR INFORMATION

Corresponding Author

Zvjezdana Findrik Blažević − *University of Zagreb Faculty of Chemical Engineering and Technology, 10 000 Zagreb, Croatia;* orcid.org/0000-0002-5312-8951; Email: zfindrik@fkit.unizg.hr

Authors

Nevena Milčić − *University of Zagreb Faculty of Chemical Engineering and Technology, 10 000 Zagreb, Croatia;* orcid.org/0000-0003-0712-2417

Martina Sudar − *University of Zagreb Faculty of Chemical Engineering and Technology, 10 000 Zagreb, Croatia*

Ana-Katarina Marić − *University of Zagreb Faculty of Chemical Engineering and Technology, 10 000 Zagreb, Croatia*

Krešimir Kos − *University of Zagreb Faculty of Chemical Engineering and Technology, 10 000 Zagreb, Croatia;* Present Address: Krešimir Kos, Shimadzu d.o.o., Zavrtnica 17, 10 000 Zagreb, Croatia

Maja Majerić Elenkov − *Division of Organic Chemistry and Biochemistry, Ruđer Bošković Institute, 10 000 Zagreb, Croatia;* orcid.org/0000-0001-6884-0928

Complete contact information is available at: https://pubs.acs.org/10.1021/acs.iecr.4c00477

Author Contributions

This manuscript was written through the contributions of all authors. All authors have given approval to the final version of the manuscript.

Funding

This work was supported by the Croatian Science Foundation (HrZZ, IP-2018-01 4493). N.M. was supported by a PhD scholarship from the Croatian Science Foundation through the Career Development Project for Young Researchers.

Notes

The authors declare no competing financial interest.

ACKNOWLEDGMENTS

The authors would like to thank Lixia Tang, PhD, for providing them a plasmid for the ISM-4 variant.

ABBREVIATIONS

1, 2-(4-fluorophenyl)oxirane; **2**, 3-(4-fluorophenyl)-3-hydroxypropanenitrile; **3**, 1-(4-fluorophenyl)-1,2-ethanediol; DMSO, dimethyl sulfoxide; EDTA, ethylenediaminetetraacetic acid; EtOAc, ethyl acetate; FID, flame ionization detector; HHDH, halohydrin dehalogenase; *i*-PrOH, isopropanol; ISM-4, HHDH variant obtained by four rounds of iterative saturation mutagenesis; MeCN, acetonitrile; MeOH, methanol; PNSHH, *para*-nitro-2- bromo-1-phenylethanol; PNSO, *para*-nitro styrene oxide; RBR, rotating-bed reactor; SDS-PAGE, sodium dodecyl-sulfate polyacrylamide gel electrophoresis; TFA, trifluoroacetic acid; Tris, tris(hydroxymethyl)aminomethane; UPW, ultrapure water

REFERENCES

(1) Tredwell, M.; Gouverneur, V. *1.5 Fluorine in Medicinal Chemistry: Importance of Chirality*; Elsevier, 2012; pp 70−85.

(2) Perrone, M. G.; Vitale, P.; Panella, A.; Tolomeo, A.; Scilimati, A. Current and Emerging Applications of Fluorine in Medicinal Chemistry. In *AD Westwell, Fluorinated Pharmaceuticals: Advances in Medicinal Chemistry*; Future Science: London, 2015; pp 126−139.

(3) Lei, A.; Liu, W. 7.13 Directed Aryl CH Oxidations with Transition Metals. In *Comprehensive Organic Synthesis*; Elsevier, 2014; pp 313−346.

(4) Šunjic, V.; Parnham, M. Signposts to Chiral Drugs. In *Organic Synthesis in Action*; Springer, 2011.

(5) Hammond, R. J.; Poston, B. W.; Ghiviriga, I.; Feske, B. D. Biocatalytic Synthesis towards Both Antipodes of 3-Hydroxy-3-Phenylpropanitrile a Precursor to Fluoxetine, Atomoxetine and Nisoxetine. *Tetrahedron Lett.* **2007**, *48* (7), 1217−1219.

(6) Müller, M. Chemoenzymatic Synthesis of Building Blocks for Statin Side Chains. *Angew. Chem., Int. Ed.* **2005**, *44* (3), 362−365.

(7) Bergeron, S.; Chaplin, D. A.; Edwards, J. H.; Ellis, B. S. W.; Hill, C. L.; Holt-Tiffin, K.; Knight, J. R.; Mahoney, T.; Osborne, A. P.; Ruecroft, G. Nitrilase-Catalysed Desymmetrisation of 3-Hydroxyglutaronitrile: Preparation of a Statin Side-Chain Intermediate. *Org. Process Res. Dev.* **2006**, *10* (3), 661−665.

(8) Kamal, A.; Khanna, G. B. R.; Ramu, R. Chemoenzymatic Synthesis2 of Both Enantiomers of Fluoxetine, Tomoxetine and Nisoxetine: Lipase-Catalyzed Resolution of 3-Aryl-3-Hydroxypropanenitriles. *Tetrahedron: Asymmetry* **2002**, *13* (18), 2039−2051, DOI: 10.1016/S0957-4166(02)00537-2.

(9) Gillis, E. P.; Eastman, K. J.; Hill, M. D.; Donnelly, D. J.; Meanwell, N. A. Applications of Fluorine in Medicinal Chemistry. *J. Med. Chem.* **2015**, *58* (21), 8315−8359.

(10) Palumbo Piccionello, A.; Pibiri, I.; Buscemi, S.; Pace, A. Recent Development in Fluorinated Antibiotics. In *Fluorine in Life Sciences: Pharmaceuticals, Medicinal Diagnostics, and Agrochemicals*; Elsevier, 2019; pp 213−239.

(11) Liang, T.; Neumann, C. N.; Ritter, T. Introduction of Fluorine and Fluorine-Containing Functional Groups. *Angew. Chem., Int. Ed.* **2013**, *52* (32), 8214−8264.
(12) Koopmeiners, J.; Halmschlag, B.; Schallmey, M.; Schallmey, A. Biochemical and Biocatalytic Characterization of 17 Novel Halohydrin Dehalogenases. *Appl. Microbiol. Biotechnol.* **2016**, *100*, 7517−7527.
(13) Schallmey, A.; Schallmey, M. Recent Advances on Halohydrin Dehalogenases—from Enzyme Identification to Novel Biocatalytic Applications. *Appl. Microbiol. Biotechnol.* **2016**, *100* (18), 7827−7839.
(14) Findrik Blažević, Z.; Milčić, N.; Sudar, M.; Majerić Elenkov, M. Halohydrin Dehalogenases and Their Potential in Industrial Application − A Viewpoint of Enzyme Reaction Engineering. *Adv. Synth. Catal.* **2021**, *363* (2), 388−410, DOI: 10.1002/adsc.202000984.
(15) Calderini, E.; Wessel, J.; Süss, P.; Schrepfer, P.; Wardenga, R.; Schallmey, A. Selective Ring-Opening of Di-Substituted Epoxides Catalysed by Halohydrin Dehalogenases. *ChemCatChem* **2019**, *11* (8), 2099−2106.
(16) Majerić Elenkov, M.; Tang, L.; Hauer, B.; Janssen, D. B. Sequential Kinetic Resolution Catalyzed by Halohydrin Dehalogenase. *Org. Lett.* **2006**, *8* (19), 4227−4229.
(17) Zhang, F.-R.; Wan, N.-W.; Ma, J.-M.; Cui, B.-D.; Han, W.-Y.; Chen, Y.-Z. Enzymatic Kinetic Resolution of Bulky Spiro-Epoxyoxindoles via Halohydrin Dehalogenase-Catalyzed Enantio- and Regioselective Azidolysis. *ACS Catal.* **2021**, *11* (15), 9066−9072.
(18) Xu, Q.; Huang, K.-S.; Wang, Y.-F.; Wang, H.-H.; Cui, B.-D.; Han, W.-Y.; Chen, Y.-Z.; Wan, N.-W. Stereodivergent Synthesis of Epoxides and Oxazolidinones via the Halohydrin Dehalogenase-Catalyzed Desymmetrization Strategy. *ACS Catal.* **2022**, *12* (11), 6285−6293.
(19) Ma, S. K.; Gruber, J.; Davis, C.; Newman, L.; Gray, D.; Wang, A.; Grate, J.; Huisman, G. W.; Sheldon, R. A. A Green-by-Design Biocatalytic Process for Atorvastatin Intermediate. *Green Chem.* **2010**, *12* (1), 81−86.
(20) Suzuki, T.; Kasai, N. Generation of Optically Active Glycerol Derivatives by Microbial Resolution - For Development of Useful Synthetic Units for Pharmaceuticals. *Trends Glycosci. Glycotechnol.* **2003**, *15* (86), 329−349, DOI: 10.4052/tigg.15.329.
(21) Song, Z.; Zhang, Q.; Wu, W.; Pu, Z.; Yu, H. Rational Design of Enzyme Activity and Enantioselectivity. *Front. Bioeng. Biotechnol.* **2023**, *11*, 1129149 DOI: 10.3389/fbioe.2023.1129149.
(22) Hall, M. Enzymatic Strategies for Asymmetric Synthesis. *RSC Chem. Biol.* **2021**, *2* (4), 958−989.
(23) Wu, Z.; Deng, W.; Tong, Y.; Liao, Q.; Xin, D.; Yu, H.; Feng, J.; Tang, L. Exploring the Thermostable Properties of Halohydrin Dehalogenase from *Agrobacterium Radiobacter* AD1 by a Combinatorial Directed Evolution Strategy. *Appl. Microbiol. Biotechnol.* **2017**, *101*, 3201−3321.
(24) Milčić, N.; Švaco, P.; Sudar, M.; Tang, L.; Findrik Blažević, Z.; Majerić Elenkov, M. Impact of Organic Solvents on the Catalytic Performance of Halohydrin Dehalogenase. *Appl. Microbiol. Biotechnol.* **2023**, *107* (7), 2351−2361.
(25) Vasić-Rački, Đ.; Findrik, Z.; Vrsalović Presečki, A. Modelling as a Tool of Enzyme Reaction Engineering for Enzyme Reactor Development. *Appl. Microbiol. Biotechnol.* **2011**, *91* (4), 845−856.
(26) Milčić, N.; Ćevid, I.; Çakar, M. M.; Sudar, M.; Blažević, Z. F. Enzyme Reaction Engineering as a Tool to Investigate the Potential Application of Enzyme Reaction Systems. *Hung. J. Ind. Chem.* **2022**, *50*, 45−55, DOI: 10.33927/hjic-2022-08.
(27) Bian, C.; Zhou, Y.-N.; Deetz, J. D.; Luo, Z.-H. Experimental and Computational Investigation of Oxidative Quenching Governed Aqueous Organocatalyzed Atom Transfer Radical Polymerization. *Chem. Eng. J.* **2019**, *362*, 721−730.
(28) Bian, C.; Zhou, Y.-N.; Guo, J.-K.; Luo, Z.-H. Aqueous Metal-Free Atom Transfer Radical Polymerization: Experiments and Model-Based Approach for Mechanistic Understanding. *Macromolecules* **2018**, *51* (6), 2367−2376.
(29) Lutje Spelberg, J. H.; Tang, L.; van Gelder, M.; Kellogg, R. M.; Janssen, D. B. Exploration of the Biocatalytic Potential of a Halohydrin Dehalogenase Using Chromogenic Substrates. *Tetrahedron: Asymmetry* **2002**, *13* (10), 1083−1089.
(30) Dokli, I.; Milčić, N.; Marin, P.; Miklenić, M. S.; Sudar, M.; Tang, L.; Findrik Blažević, Z.; Majerić Elenkov, M. Halohydrin Dehalogenase-Catalysed Synthesis of Fluorinated Aromatic Chiral Building Blocks. *Catal. Commun.* **2021**, *152*, No. 106285.
(31) Pedragosa-Moreau, S.; Morisseau, C.; Zylber, J.; Archelas, A.; Baratti, J.; Furstoss, R. Microbiological Transformations. 33. Fungal Epoxide Hydrolases Applied to the Synthesis of Enantiopure Para-Substituted Styrene Oxides. A Mechanistic Approach. *J. Org. Chem.* **1996**, *61* (21), 7402−7407.
(32) Bradford, M. M. A Rapid and Sensitive Method for the Quantitation of Microgram Quantities of Protein Utilizing the Principle of Protein-Dye Binding. *Anal. Biochem.* **1976**, *72* (1), 248−254.
(33) Fischer Scientific. https://www.fishersci.at. (accessed Sep 27, 2023).
(34) Milčić, N.; Stepanić, V.; Crnolatac, I.; Findrik Blažević, Z.; Brkljača, Z.; Majerić Elenkov, M. Inhibitory Effect of DMSO on Halohydrin Dehalogenase: Experimental and Computational Insights into the Influence of an Organic Co-Solvent on the Structural and Catalytic Properties of a Biocatalyst. *Chem. - Eur. J.* **2022**, *28* (56), No. e202201923, DOI: 10.1002/chem.202201923.
(35) Milčić, N.; Sudar, M.; Dokli, I.; Majerić Elenkov, M.; Findrik Blažević, Z. Halohydrin Dehalogenase-Catalysed Synthesis of Enantiopure Fluorinated Building Blocks: Bottlenecks Found and Explained by Applying a Reaction Engineering Approach. *React. Chem. Eng.* **2023**, *8* (3), 673−686.
(36) SCIENTIST Handbook *Micromath, Salt Lake City,* 1986−1995.
(37) Fraser, J.; Bickerstaff, G. Entrapment in Calcium Alginate. In *Immobilization of Enzymes and Cells*; Humana Press, 2008; pp 61−66.
(38) Findrik, Z.; Vasić-Rački, Đ. Mathematical Modelling of Amino Acid Resolution Catalyzed by L-Amino Acid Oxidases from *Crotalus Adamanteus* and *Crotalus Atrox*. *Process Biochem.* **2008**, *43* (11), 1186−1194, DOI: 10.1016/j.procbio.2008.06.010.
(39) Wang, X.; Han, S.; Yang, Z.; Tang, L. Improvement of the Thermostability and Activity of Halohydrin Dehalogenase from *Agrobacterium Radiobacter* AD1 by Engineering C-Terminal Amino Acids. *J. Biotechnol.* **2015**, *212*, 92−98.
(40) Wang, X.; Lin, H.; Zheng, Y.; Feng, J.; Yang, Z.; Tang, L. MDC-Analyzer-Facilitated Combinatorial Strategy for Improving the Activity and Stability of Halohydrin Dehalogenase from *Agrobacterium Radiobacter* AD1. *J. Biotechnol.* **2015**, *206*, 1−7.
(41) Schallmey, M.; Floor, R. J.; Hauer, B.; Breuer, M.; Jekel, P. A.; Wijma, H. J.; Dijkstra, B. W.; Janssen, D. B. Biocatalytic and Structural Properties of a Highly Engineered Halohydrin Dehalogenase. *ChemBioChem* **2013**, *14* (7), 870−881.
(42) Koopmeiners, J.; Diederich, C.; Solarczek, J.; Voß, H.; Mayer, J.; Blankenfeldt, W.; Schallmey, A. HheG, a Halohydrin Dehalogenase with Activity on Cyclic Epoxides. *ACS Catal.* **2017**, *7*, 6877−6886.
(43) Vasić-Rački, Đ.; Bongs, J.; Schörken, U.; Sprenger, G.; Liese, A. Modeling of Reaction Kinetics for Reactor Selection in the Case of L-Erythrulose Synthesis. *Bioprocess. Biosyst. Eng.* **2003**, *25*, 285−290.
(44) Česnik, M.; Sudar, M.; Roldan, R.; Hernandez, K.; Parella, T.; Clapés, P.; Charnock, S.; Vasić-Rački, Đ.; Findrik Blažević, Z. Model-Based Optimization of the Enzymatic Aldol Addition of Propanal to Formaldehyde: A First Step towards Enzymatic Synthesis of 3-Hydroxybutyric Acid. *Chem. Eng. Res. Des.* **2019**, *150*, 140−152.
(45) Baslé, E.; Joubert, N.; Pucheault, M. Protein Chemical Modification on Endogenous Amino Acids. *Chem. Biol.* **2010**, *17* (3), 213−227.
(46) Mateo, C.; Torres, R.; Fernández-Lorente, G.; Ortiz, C.; Fuentes, M.; Hidalgo, A.; López-Gallego, F.; Abian, O.; Palomo, J. M.; Betancor, L.; Pessela, B. C. C.; Guisan, J. M.; Fernández-Lafuente, R. Epoxy-Amino Groups: A New Tool for Improved Immobilization of Proteins by the Epoxy Method. *Biomacromolecules* **2003**, *4* (3), 772−777.

(47) Faber, K. Biocatalytic Applications. In *Biotransformations in Organic Chemistry: A Textbook*; Faber, K., Ed.; Springer Berlin Heidelberg: Berlin, Heidelberg, 2011; pp 31−313.
(48) Tufvesson, P.; Lima-Ramos, J.; Nordblad, M.; Woodley, J. M. Guidelines and Cost Analysis for Catalyst Production in Biocatalytic Processes. *Org. Process Res. Dev* **2011**, *15* (1), 266−274.
(49) Solarczek, J.; Kaspar, F.; Bauer, P.; Schallmey, A. G-Type Halohydrin Dehalogenases Catalyze Ring Opening Reactions of Cyclic Epoxides with Diverse Anionic Nucleophiles. *Chem. - Eur. J.* **2022**, *28* (72), No. e202202343, DOI: 10.1002/chem.202202343.
(50) An, M.; Liu, W.; Zhou, X.; Ma, R.; Wang, H.; Cui, B.; Han, W.; Wan, N.; Chen, Y. Highly α-Position Regioselective Ring-Opening of Epoxides Catalyzed by Halohydrin Dehalogenase from *Ilumatobacter Coccineus*: A Biocatalytic Approach to 2-Azido-2-Aryl-1-Ols. *RSC Adv.* **2019**, *9* (29), 16418−16422.
(51) Majerić Elenkov, M.; Primožič, I.; Hrenar, T.; Smolko, A.; Dokli, I.; Salopek-Sondi, B.; Tang, L. Catalytic Activity of Halohydrin Dehalogenases towards Spiroepoxides. *Org. Biomol. Chem.* **2012**, *10*, 5063−5072.
(52) Majerić Elenkov, M.; Čičak, M.; Smolko, A.; Knežević, A. Halohydrin Dehalogenase-Catalysed Transformations of Epifluorohydrin. *Tetrahedron Lett.* **2018**, *59* (4), 406−408.
(53) Spinchem. https://www.spinchem.com/. (accessed Sep 21, 2023).
(54) Milker, S.; Fink, M. J.; Oberleitner, N.; Ressmann, A. K.; Bornscheuer, U. T.; Mihovilović, M. D.; Rudroff, F. Kinetic Modeling of an Enzymatic Redox Cascade In Vivo Reveals Bottlenecks Caused by Cofactors. *ChemCatChem* **2017**, *9* (17), 3420−3427.
(55) Česnik Katulić, M.; Sudar, M.; Hernández, K.; Qi, Y.; Charnock, S. J.; Vasić-Rački, Đ.; Clapés, P.; Findrik Blažević, Z. Cascade Synthesis of L-Homoserine Catalyzed by Lyophilized Whole Cells Containing Transaminase and Aldolase Activities: The Mathematical Modeling Approach. *Ind. Eng. Chem. Res.* **2021**, *60* (38), 13846−13858, DOI: 10.1021/acs.iecr.1c02343.